Computers in Biology and Medicine 114 (2019) 103440

Contents lists available at ScienceDirect

Computers in Biology and Medicine

journal homepage: http://www.elsevier.com/locate/compbiomed

Calculation of the aortic arch angles from three-dimensional reconstructions of computed tomography scans: Comparison between an automated program and visual assessment

Julien Gaudric [a,d,1], María Teresa Politi [b,c,1,*], Juan Manuel Fernández [b,c], Emmanuelle Carre [d], Claudia Capurro [b,c], José María Fullana [d]

[a] Service de Chirurgie Vasculaire, Hôpitaux Universitaires La Pitié-Salpêtrière, 47-83 Bd del'Hôpital, 75013, Paris, France
[b] Universidad de Buenos Aires, Facultad de Medicina. Departamento de Ciencias Fisiológicas, Laboratorio de Biomembranas, Paraguay 2155, C1121 ABG, Buenos Aires, Argentina
[c] CONICET-Universidad de Buenos Aires. Instituto de Fisiología y Biofísica Bernardo Houssay, Paraguay 2155, C1121 ABG, Buenos Aires, Argentina
[d] Sorbonne Université, UPMC UnivParis06, CNRS, UMR7190, Institut Jean Le Rond d'Alembert, 75005, Paris, France

ARTICLE INFO

Keywords:
Multidetector computed tomography
Thoracic aorta
Thoracic aortic aneurysm
Reproducibility
Validation studies

ABSTRACT

Background: The curvature of the aortic arch is associated with the risk of endoleak formation after thoracic endovascular aortic repair (TEVAR). However, the adequate assessment of the angles of the aorta continues to represent a major difficulty. We developed a new program based on three-dimensional (3D) reconstructions of computed tomography (CT) scans to objectively identify the location of the aortic points of maximum curvature, and to automatically calculate the main aortic arch angles, comparing final values with visual assessment methods.

Methods: This is a cross-sectional validation study of a convenience sample of subjects with multislice CT angiography scans of the thoracic aorta from an institutional imaging database. The center lumen line (CLL) of the aorta was determined semi-automatically using Endosize software. The points of maximum curvature on the CLL were determined by two methods: visually by two physicians and through a custom program.

Results: The study enrolled 9 subjects: 4 with thoracic aneurysms and 5 with normal aortas. The inter-observer and inter-method correlation, agreement and reliability for each of the 3D spatial coordinates of the points of maximum curvature were appropriate. However, the aortic angles determined by visual assessment showed a very low to moderate correlation and reliability with those determined by our custom program.

Conclusion: An automated custom program can reflect clinician's intuitive assessment of the location of points of maximum curvature and translate it into aortic angles with an apparently higher precision, reducing potential error and user time.

1. Background

The aorta is a complex structure that changes drastically in patients with aneurysmal diseases. Three dimensional (3D) computed tomography (CT) scans are currently the most widely used imaging modality for evaluating aortic geometry [1,2]. However, the appropriate characterization of its size and shape in both normal and diseased settings still remains a challenge.

Though there is a wealth of information indicating that the morphology of the abdominal aorta is an important predictor of clinical outcomes, data on the thoracic aorta are still scarce [3,4]. There is evidence that the location and tortuosity of the aorta may be related to the risk of endoleak formation after thoracic endovascular aortic repair (TEVAR) [5–7]. The magnitude of aortic angles, especially in the proximal and distal neck, and the radius of the aortic arch curvature may also increase the risk of endoleaks [8,9]. However, both in research and in

* Corresponding author. Laboratorio de Biomembranas Departamento de Ciencias Fisiológicas Facultad de Medicina Universidad de Buenos Aires Paraguay 2155, C1121 ABG, Buenos Aires, Argentina.
E-mail addresses: jgaudric@gmail.com (J. Gaudric), mpoliti@fmed.uba.ar (M.T. Politi), jmfbur@gmail.com (J.M. Fernández), emmanuelle.manou@gmail.com (E. Carre), capurroclaudia@yahoo.com.ar (C. Capurro), jose.fullana@upmc.fr (J.M. Fullana).
[1] Both authors contributed equally.

https://doi.org/10.1016/j.compbiomed.2019.103440
Received 3 January 2019; Received in revised form 6 September 2019; Accepted 7 September 2019
Available online 9 September 2019

current clinical practice, the points of maximum curvature of the aorta are usually assessed visually at the risk of inaccuracies, high inter-observer variance and prolonged user time [10,11]. Though several automated methods have been proposed to accurately measure the curvature of the thoracic aorta, many rely on global indicators of curvature or on geometric assumptions and have not been formally compared to visual assessment methods [12–14]. In this validation study we propose a new automated program to objectively identify the precise location of the aortic points of maximum curvature and, without relying on geometric assumptions, to automatically calculate the angles of the thoracic aorta, comparing final values with visual assessment methods. We believe that such a program could potentially be useful in the clinical workup of patients with thoracic aneurysms, to identify patients at risk for endoleak formation after TEVAR.

2. Methods

2.1. Study design and image acquisition

This is a cross-sectional, observational study of a convenience sample of CT angiography scans of the thoracic aorta collected retrospectively from the institutional imaging database of the Vascular Surgery Department of the *Hôpitaux Universitaires La Pitié-Salpêtrière* in Paris, France. Patients were classified into two groups according to the final report on the CT scan: one with thoracic aorta aneurysms and another with normal healthy aortas.

CT angiography scans of the aorta were taken using the peripheral intravenous injection of iodinated contrast agent at arterial phase. The optimization of intra-luminal enhancement during peak aortic opacification was obtained by automated bolus tracking. CT images were acquired using multislice CT scans and Digital Imaging Communication in Medicine (DICOM) data with a maximum slice thickness of 3 mm and a minimum reconstruction interval of 1 mm. CT scans were synchronized with electrocardiogram gating to avoid beating artifacts and were required to include the entire thoracic aorta from the coronary arteries to the coeliac trunk. Images were anonymized to preserve patient confidentiality.

2.2. Extraction of the center lumen line

Three-dimensional (3D) reconstructions of the thoracic aorta using segmentation and volume rendering techniques were generated using an automatic 3D sizing Endosize software (Therenva, Rennes, France) that is commercially available [15–17]. The center lumen line (CLL) of each vessel was determined semi-automatically from CT angiography scans of the aorta using Endosize software. The 3D coordinates of the first and last points of the CLL were manually identified by visual assessment by two trained physicians (JMF and MTP) in order to generate a CLL of the entire thoracic aorta. The first point of the CLL corresponds to the cross section passing through the ostium of the right coronary artery and the last one corresponds to the cross section passing through the coeliac trunk. The mean of each axis position was then calculated for each point, obtaining a mean first point and a mean last point. The rest of the CLL points were automatically generated by Endosize software using these two points. This CLL was used thereon for identifying the points of maximum curvature by two different methods: visual assessment and by using a custom program. Visual assessment of points of maximum curvature was done using Endosize software. The identification of points of maximum curvature using our custom program required extracting the 3D coordinates of each point on the CLL from Endosize software.

2.3. Identification of points of maximum curvature by visual assessment

The 3D coordinates of points of maximum curvature were identified by visual assessment using combined volume rendering images overlapping CLL tracings on aortic 3D CT angiograms created by Endosize software (Fig. 1). This was done by two trained physicians (JMF and MTP) using a standardized method that has been previously described and validated [10,11]. Briefly, after 3D image reconstruction, the aorta was turned 360° perpendicular to the center of the CLL and then rotated along its longitudinal axis, until the sharpest angle was identified. The vertex of this angle was considered the point of maximum curvature by visual assessment. The amount of points of maximum curvature identified visually was established following the observers' criteria; there was not a fixed amount of points pre-specified. All points of maximum curvature were selected independently by each operator on two different occasions separated two weeks apart, as to evaluate both interobserver and intraobserver variability.

2.4. Identification of points of maximum curvature by custom program

The points of maximum curvature were also identified automatically using our custom program developed in MATLAB (R2018a, The MathWorks, Inc., Natick, Massachusetts). After importing the 3D coordinates of the CLL from the Endosize software, each point on the CLL was identified using our custom program following a parametric approach r(s)=(x(s),y(s),z(s)) where *s* is the parameter running from the first point (considered as 1) to the last point of the line and therefore represents the length of the aorta. The calculation of x(s), y(s), z(s) and their derivatives was done by spline interpolation between neighboring points given a parametric curve, which also allowed to compute the derivatives using s as a parameter. The first derivatives were computed as the first order difference for a vector X with points separated by Δ (which is equal to 1 because it deals with parametric deviation). That is:

$$\left[\frac{x(2)-x(1)}{\Delta}, \frac{x(3)-x(2)}{\Delta}, \ldots, \frac{x(n)-x(n-1)}{\Delta}\right] \quad (1)$$

The second derivatives were found simply by applying the first derivatives to the resulting vector. The curvature radius k was computed following the equation:

$$k = \frac{r' \chi\, r''}{r'^3} \quad (2)$$

where r' and r'' stand for the first and second derivatives of the function r(s) and the cross (χ) denotes the vector cross product. The norm of the vector is symbolized as ||.|| and is defined as the square root of the sum of the values of the x, y and z spatial coordinates of the vector, each raised to the second power. This is:

$$X = \sqrt{x^2 + y^2 + z^2} \quad (3)$$

To reduce the noise related to signal pixelations and transformations from the interface tool, we used a digital filter where the output is a clean *r_c(s)* signal that is the result of the convolution of its input *r(s)* with a unit-average impulse response *h(s)*. Equation (2) was then applied to the CLL, generating a function of the curvature radius *k* over the aortic length (or position) (Fig. 1, right image). The points with a radius curvature over a threshold of 0.2 cm^{-1} were identified, following previous studies that suggest that thoracic aorta curvature values above this threshold correspond to the main aortic angulations [5,6]. This threshold allowed to distinguish areas of high curvature values (>0.2 cm^{-1}) that were separated by areas of low curvature values (<0.2 cm^{-1}). The point with the highest curvature value within each individual area of high curvature values was considered the point of maximum curvature for that area. Hence, all points of maximum curvature on a specific thoracic aorta were identified. Again, there was not a fixed amount of points pre-specified. The 3D coordinates of these points were automatically generated and compared for correlation and agreement with the points determined by visual assessment by each operator.

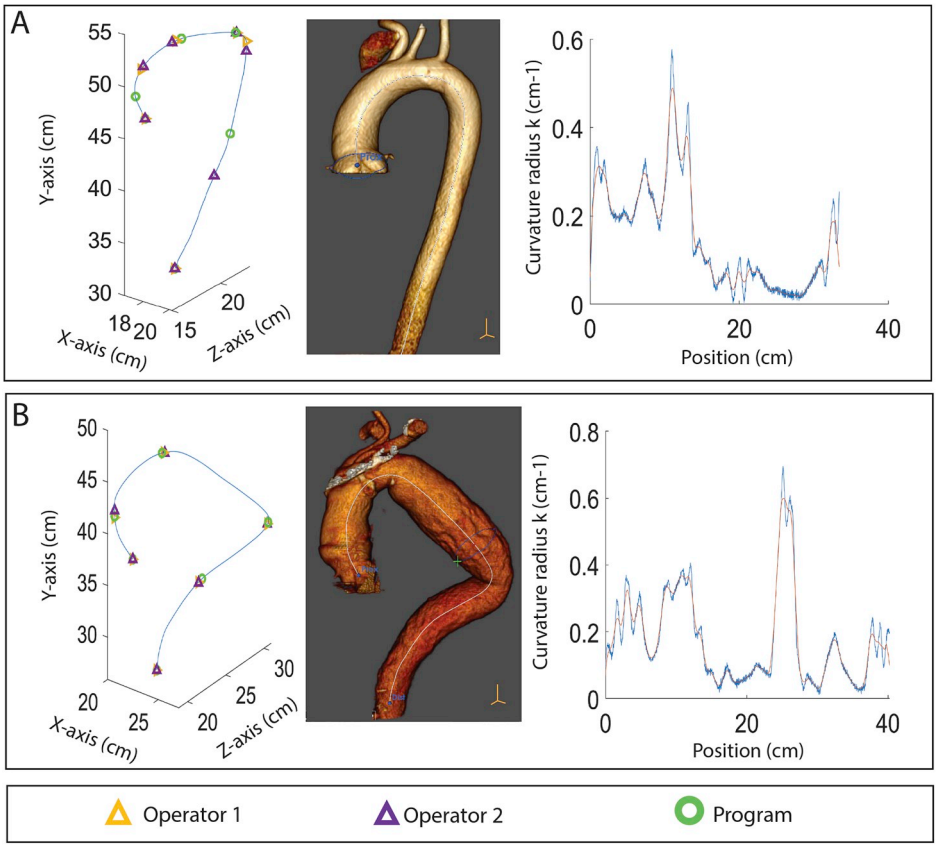

Fig. 1. Imaging analysis of representative subjects with a normal aorta (A) or a thoracic aneurysm (B). *Left image:* Two-dimensional (2D) plot of the three dimensional (3D) skeletonized aortic center lumen line (CLL) generated semi-automatically by Endosize software. The points of maximum curvature identified by each operator/method are indicated. *Middle image:* CT angiography scans of aortic vessels. Cardiac structures were removed using Endosize software. The CLL was semi-automatically determined by Endosize software. *Right image:* Plot of curvature radius k (cm^{-1}) over position obtained from program analysis of the CLL. Blue line represents raw data. Yellow line represents data from applying Equation (2).

2.5. Aortic angle calculations

The three datasets of points of maximum curvature (*i.e.*, those identified by visual assessment by each operator and those estimated using a custom program) were imported into our custom program in MATLAB and used to calculate the aortic angles (*i.e.*, the angles between the straight lines that join the points of maximum curvature) (Fig. 2A). To do so, from each set of points of maximum curvature, we selected three consecutive points and connected them with two straight lines or vectors (X_1 and X_2). The aortic angle at the point of intersection between two vectors was defined as the dot product between those two vectors:

$$X_1 . X_2 = \|X_1\| \|X_2\| cos\ \Theta \quad 4$$

This same process was repeated for all three consecutive points of maximum curvature in each of the three datasets.

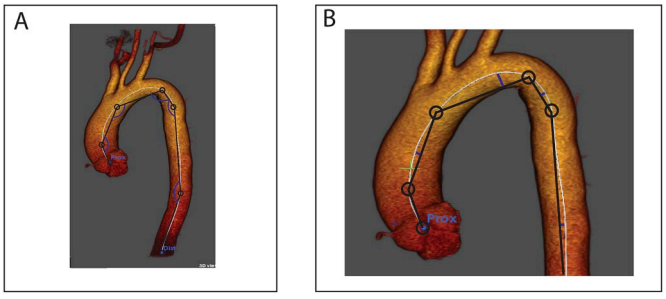

Fig. 2. Scheme representing how aortic angles (A) and algebraic distances (B) were calculated. A. Given a dataset of points of maximum curvature (in this representative figure, the black circles), three consecutive points of maximum curvature were selected. These points were connected with two straight lines or vectors (black lines). The angle at the point of intersection between the two vectors was considered the aortic angle (blue arches). B. Close-up of previous image. The algebraic distance between the center lumen line (CLL) and the straight lines for each dataset was defined as the maximum length of a line that perpendicularly intersects both the CLL and each straight line between points of maximum curvature (*i.e.,* that crosses these lines at a right angle (90°). In this representative figure, the algebraic distances are the straight blue lines.

2.6. Algebraic distance between the CLL and straight lines between points of maximum curvature

To estimate the accuracy with which the straight lines between the points of maximum curvature represent a simplified version of the CLL (so that most of the information on the CLL would be contained in just a few points), we calculated in MATLAB an algebraic measure between the CLL and the straight lines for each of the three datasets (Fig. 2B). Given that the thoracic aorta does not have any major changes in its concavity throughout its path, this measure was defined as the maximum length of a line that perpendicularly intersects both the CLL and each straight line between points of maximum curvature (*i.e.*, that crosses these lines at a right angle (90°)). The algebraic measures between the CLL and the straight lines for each operator/method were then compared against each other for both normal aortas and thoracic aneurysms.

2.7. Calculation of aortic curvature, tortuosity index and curvature-length index

To further characterize the geometry of thoracic aneurysms, we analyzed the association between different indicators of aortic curvature and the presence of aneurysms. These indicators were calculated using the function curvature radius *k* over the aortic length (or position) (Fig. 1, right image) generated by applying Equation (2) to the CLL using our custom program. The three indicators calculated from this function were: the aortic curvature [cm^{-1}] (*i.e.*, the integral of the CLL curvature

as a function of the length of the aorta divided by the length of the aorta), the tortuosity index (*i.e.*, an adimensional variable that represents the relation between the length of the aorta and the minimum distance between the first and the last points of the aorta) and the aortic curvature-length index (*i.e.* an adimensional variable that represents the integral of the curvature of the CLL as a function of the length of the aorta) [18–20].

2.8. Ethical issues

This study is in accordance with the Code of Ethics of the World Medical Association (Declaration of Helsinki) for experiments involving humans. Since this is an observational study involving minimum risk to human subjects and the privacy of their personal information, the local IRB of the *Hôpitaux Universitaires La Pitié-Salpêtrière* approved this study and waived the requisite to obtain informed consent. Privacy rights of human subjects were observed through anonymization of data.

2.9. Statistical issues

An initial one-way analysis was conducted to assess the distribution for each variable. Continuous variables were summarized using mean and standard deviation (SD) for normally distributed variables and median and interquartile range (IQR) for non-normally distributed variables. Normality was assessed formally by Shapiro-Wilk tests. Categorical variables were summarized with percentages in each category.

Intra-observer, inter-observer and inter-method variability of the coordinates of the points of maximum curvature were estimated through five analyses: the discrepancy in the number of points identified by each operator/method, correlation coefficients, and Bland-Altman agreement plots, reliability coefficients, and interclass correlation coefficients. For simplicity, the last two analyses were only applied to inter-observer and inter-method variability. Furthermore, though the rest of the analyses were done by discriminating normal aortas from those with thoracic aneurysms, for clarity, Bland-Altman plots considered both types of aortas together.

Inter-observer and inter-method variabilities for aortic angles were also estimated through five analyses: correlation coefficients, mean differences, Bland-Altman agreement plots, reliability coefficients, and interclass correlation coefficients. These analyses were chosen to compare our results with previous reports in the literature [11,20]. Again, for clarity, Bland-Altman plots considered both types of aortas together; the rest of the analyses were done by separating normal aortas from those with thoracic aneurysms.

Correlation between operators/methods were assessed with Pearson's correlation coefficient (ρ) for variables with a multivariate normal distribution and with Spearman's correlation coefficient (rs) for variables with a non-normal multivariate distribution. A general scale for evaluating correlation coefficients is that values less than 0.30 represent little if any correlation, between 0.30 and 0.49 low correlation, between 0.50 and 0.69 indicate moderate correlation, between 0.70 and 0.89 indicate high correlation, and values greater than 0.90 indicate very good correlation [21]. If the amount of observations were different among comparing pairs (observers/methods), the observation with the highest Euclidean distance from the comparing observations would be considered as a separate point identified by only one observer/method and would be removed from the analysis. The discrepancy in the number of points identified by each operator/method (*i.e.*, the amount of points identified only once or only by one operator/method) was also evaluated. Since two methods can show excellent correlation despite the presence of significant systematic bias, assessment of agreement and reliability was also performed. Bland-Altman agreement plots represent the difference between two measurements on the y-axis plotted against the average of these measurements on the x-axis. The mean difference between the two measurements is called the center of agreement and is represented by a central horizontal line on the plot. The upper/lower limits of agreement are ±1.96 SD of the mean difference [22]. The gap between the center of agreement and the x-axis (corresponding to zero differences) is called the bias. Global agreement between measurements was assessed by visual examination of the Bland-Altman plots [23]. Reliability was measured with the repeatability coefficient (RC), which is defined as [11,23]:

$$RC = 1.96 * \sqrt{\frac{\sum_i^n (x_1 - x_2)^2}{n}}$$

with $(x_1 - x_2)$ being the difference between two measurements. The RC is the value below which the absolute differences between two measurements would lie with 0.95 probability. This index takes into account both random and systematic errors and therefore quantifies absolute reliability in the same units as the measurement tool [24]. Reliability was also measured with intraclass correlation coefficients (ICC) using a two-way mixed-effects model based on mean-rating following the absolute agreement definition. ICC represents the proportion of variance in data that is explained by between-rater differences [25]. Higher ICC values indicate greater reliability between the measurements of the same patient. A general guidelines is that values less than 0.50 are indicative of poor reliability, values between 0.50 and 0.75 indicate moderate reliability, values between 0.75 and 0.90 indicate good reliability, and values greater than 0.90 indicate excellent reliability [26].

Group comparisons involved two-tailed non-paired T tests for normally distributed variables, Wilcoxon (Mann-Whitney U) test for non-normally distributed variables and chi-square or Fischer's exact tests for categorical variables. A one-way analysis of variance (ANOVA) was used to determine differences between the means of three or more groups for variables with a normal distribution; a Kruskal-Wallis test was used in cases with a non-normal distribution. Two-tailed tests were considered statistically significant at the 0.05 level. When performing analyses between three or more groups, Bonferroni-adjusted alpha levels were used (following 0.05/c, being c the number of comparisons on the same dependent variable). All analyses were performed using STATA software version 15 and R software version 1.0.136 [27].

3. Results

This study included CT scans from 9 subjects: 4 with thoracic aneurysms and 5 with normal aortas. Overall, subjects were mostly middle-aged (mean: 58.4 years-old) males (67%), with no significant differences between groups.

3.1. Three-dimensional coordinates of points of maximum curvature

There was an appropriate correlation between the 3D coordinates of the first and last points of the CLL identified by two operators on each axis (Pearson's correlation, $\rho > 0.99$; $p < 0.0001$ in all cases). A mean first point and a mean last point were then obtained and used to automatically generate the rest of the CLL points using Endosize software.

For each aortic CT scan 5–7 points were obtained: 3–5 points of maximum curvature identified by at least two operators/methods, plus the first and last points that signaled the beginning and the end of the CLL (which were the same for each subject for all operators/methods). The 3D spatial coordinates of the points of maximum curvature are shown on the left side of Fig. 1 images. Overall, there were 35–36 points of maximum curvature identified by at least two operators/methods. On the aortas with aneurysms, 59% of the points of maximum curvature were on the aneurysm itself, while the rest were on the proximal landing zone.

3.1.1. Discrepancies in the number of points identified by each operator/method

When comparing points of maximum curvature identified by operators 1 and 2, there were 4 points identified by only one operator. When

comparing points of maximum curvature identified by operators 1 or 2 with those identified by the custom program, in both cases there were 7 points identified by only one method. There were no significant differences in the proportion of discrepancies between operators/methods (χ^2=0.88; p = 0.6440) (Table 1).

On repeat testing two weeks later, both operators 1 and 2 identified 35 points for the second time. In both cases, 2–3 points were identified on only one occasion. There were no significant differences in the proportion of discrepancies on repeat testing between operators (χ^2=0.14; p = 0.7130) (Table 2).

3.1.2. Correlation among points identified by different operators/methods

After removing the points identified by only one observer/method (as described in the Methods section), the inter-observer and inter-method correlation coefficients for each of the 3D spatial coordinates of the maximum curvature points were calculated using Pearson's correlation coefficient. In most cases, the correlation coefficient was very high ($\rho > 0.93$; $p < 0.0001$); for two comparisons it was high ($\rho > 0.80$; $p < 0.0001$) (one comparison applied to normal aortas and another to aortas with thoracic aneurysms) (Table 1) (Fig. 3). Intra-observer correlation was also measured following the same method, reaching appropriate results for both groups of subjects ($\rho > 0.96$; $p < 0.0001$) (Table 2) (Fig. 4).

3.1.3. Bland-Altman agreement plots of points identified by different operators/methods

Bland-Altman plots show inter-observer/method agreement and intra-observer agreement between points of maximum curvature (Figs. 5 and 6, respectively). In all comparisons, the bias was small and most of the differences between the two measurements were within the limits of agreement. There was no systematic bias identified in the distribution of mean differences across the average of these two measurements.

3.1.4. Repeatability coefficients and interclass correlation coefficients among points identified by different operators/methods

The RC and the ICC of the points of maximum curvature were evaluated for normal aortas and for thoracic aneurysms, testing both inter-observer and inter-method reliability. For both normal aortas and thoracic aneurysms, the inter-observer and inter-method RC were appropriate (*i.e.*, within 9.2% and 23.0% of the first measurement) and the inter-observer and inter-method ICC were good (in three cases, one for inter-observer reliability and two for inter-method reliability) or excellent (Table 3).

3.2. Aortic angles

The aortic angles formed by the straight lines between the points of maximum curvature identified by each operator/method were also calculated for each group of subjects in each of the three datasets.

3.2.1. Correlation among aortic angles calculated from the points of maximum curvature identified by different operators/methods

The inter-observer and inter-method correlation coefficients for each of the aortic angles were also calculated using Pearson's correlation coefficient. Hypotheses testing was conducted using a Bonferroni-adjusted alpha levels of 0.0083 in each test (0.05/6). Among subjects with thoracic aneurysms, although there was a very high and significant correlation between operators 1 and 2 ($\rho = 0.98$; $p < 0.0001$), the correlation between the operators and the program was moderate, though non-significant (operator 1: $\rho = 0.57$; $p = 0.0203$; operator 2: $\rho = 0.62$; $p = 0.0111$). Among subjects with normal aortas, there was a moderate though significant correlation between operators 1 and 2 ($\rho = 0.62$; $p = 0.006$). Between the operators and the program this correlation was very low and non-significant (operator 1: $\rho = 0.21$; $p = 0.3681$; operator 2: $\rho = 0.32$; $p = 0.1595$) (Fig. 7).

3.2.2. Bland-Altman agreement plots of aortic angles calculated from the points of maximum curvature identified by different operators/methods

Bland-Altman plots show inter-observer/method agreement for aortic angles. In all comparisons, the bias was small and most of the differences between the two measurements were within the limits of agreement. There was no systematic bias identified in the distribution of mean differences across the average of these two measurements. Overall, the inter-method variability was higher than the inter-observer variability for both normal aortas and aortas with thoracic aneurysms. This result can be visualized by a wider range of the limits of agreement (*i.e.*, ±1.96 SD of the mean difference) in the Bland-Altman plots comparing the program with an operator and those comparing operators among each other (Fig. 8).

3.2.3. Mean differences among aortic angles calculated from the points of maximum curvature identified by different operators/methods

In both subjects with and without thoracic aneurysms, the mean values of the aortic angles calculated from the points of maximum curvature identified by the program were non-significantly higher than those calculated from the points of maximum curvature identified visually (thoracic aneurysms: $124.3 \pm 32.8^\circ$ vs $117.0 \pm 30.4^\circ$, $p = 0.4282$; normal aortas: $131.8 \pm 24.7^\circ$ vs $127.5 \pm 26.5^\circ$, $p = 0.5281$). There were also no significant differences between operators in either group of subjects (thoracic aneurysms: $p = 0.7104$; normal aortas: $p = 0.8374$) (ANOVA: $F = 0.49$; $p = 0.6114$) (Tables 4 and 5).

3.2.4. Repeatability coefficients and interclass correlation coefficients among aortic angles calculated from the points of maximum curvature identified by different operators/methods

The RC of the aortic angles were evaluated for normal aortas and for thoracic aneurysms, testing both inter-observer and inter-method reliability. For both normal aortas and thoracic aneurysms the inter-observer RC were appropriate (32.6° [25.9%] and 29.7° [25.1%], respectively). However the inter-method RC for both normal aortas and

Table 1
Inter-observer and inter-method correlation of three-dimensional (3D) spatial coordinates of points of maximum curvature measured by two different operators and by a custom program in subjects with normal aortas or thoracic aneurysms. Correlation is presented using Pearson's correlation coefficient (ρ) for each axis. * p-value <0.0001. ⌈ Operators 1 vs 2: discrepancy in 1 point from an aorta with a thoracic aneurysm and 3 from normal aortas; $\chi^2 = 0.56$; $p = 0.4555$. ⁋ Operator 1 vs program: discrepancies in 4 points from aortas with thoracic aneurysms and in 3 points from normal aortas; $\chi^2 = 0.38$; $p = 0.5377$. ‖Operator 2 vs program: discrepancies in 3 points from aortas with thoracic aneurysms and in 4 points from normal aortas; $\chi^2 = 0.01$; $p = 0.9383$). There were no significant differences in the proportion of discrepancies between operators/methods ($\chi^2 = 0.88$; $p = 0.6440$). Hypotheses testing was conducted using a Bonferroni-adjusted alpha level of 0.0083 in each test (0.05/6).

	Type of aorta	x-axis ρ	y-axis ρ	z-axis ρ	Points removed	Points identified by both observers/methods
Operator 1 vs. Operator 2⌈	Normal	0.9387*	0.9712*	0.8086*	3	19
	Aneurysm	0.9728*	0.9838*	0.9735*	1	16
Operator 1 vs. Program⁋	Normal	0.9725*	0.9993*	0.9633*	3	20
	Aneurysm	0.9388*	0.9748*	0.9495*	4	16
Operator 2 vs. Program ‖	Normal	0.9715*	0.9897*	0.9862*	4	20
	Aneurysm	0.8981*	0.9456*	0.9784*	3	16

Table 2
Intra-observer correlation of three-dimensional (3D) spatial coordinates of points of maximum curvature measured twice by the same operator two weeks apart, in both subjects with normal aortas and with thoracic aneurysms. Correlation is presented using Pearson's correlation coefficient (ρ) for each axis. * p-value <0.0001. ⌠ Operator 1: discrepancies in 3 points, all from normal aortas; $\chi^2 = 2.64$; $p = 0.1044$ ⁇ Operator 2: discrepancy in 1 point from an aorta with a thoracic aneurysm and in 1 point from a normal aorta; $\chi^2 = 0.02$; $p = 0.9003$. There were no significant differences in the proportion of discrepancies on repeat testing between operators ($\chi^2 = 0.14$; $p = 0.7130$). Hypotheses testing was conducted using a Bonferroni-adjusted alpha level of 0.0125 in each test (0.05/4).

A	Type of aorta	x-axis ρ	y-axis ρ	z-axis ρ	Points removed	Points identified on both measurements
Operator 1	Normal	0.9715*	0.9897*	0.9862*	3⌠	18
	Aneurysm	0.9845*	0.9958*	0.8034*	0	17
Operator 2	Normal	0.8414*	0.9504*	0.9986*	1⁇	19
	Aneurysm	0.9979*	0.9977*	0.9971*	1	16

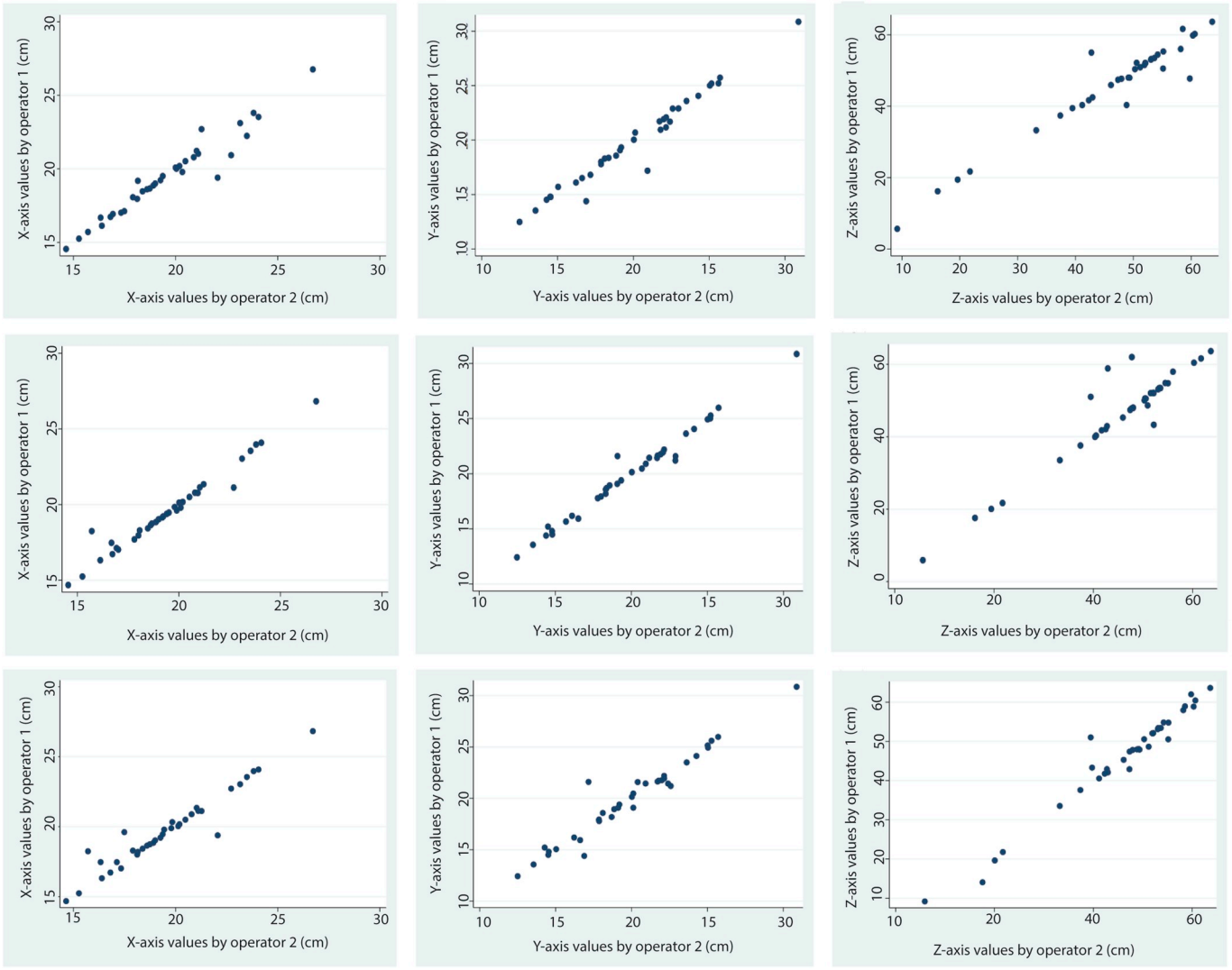

Fig. 3. Two-way scatter plots of inter-observer and inter-method correlations for all points of maximum curvature (from both subjects with normal aortas and with thoracic aneurysms). *First row:* Inter-observer correlations between operators 1 and 2. *Second row:* Inter-method correlations between program and operator 1. *Third row:* Inter-method correlation between program and operator 2. *First column:* X-axis values. *Second column:* Y-axis values. *Third column:* Z-axis values.

thoracic aneurysms were moderately high (54.9 [41.6%] and 45.0 [36.2%], respectively), indicating a greater variance between the angles measured by the program and by visual assessment. The ICC of the aortic angles were also evaluated for normal aortas and for thoracic aneurysms, testing both inter-observer and inter-method reliability. For both normal aortas and thoracic aneurysms the inter-observer ICC were good (0.87) and excellent (0.93), respectively. However the inter-method ICC were poor (0.49) and moderate (0.82), respectively, once again suggesting a greater variance between the angles measured by the program and by visual assessment (Table 5).

3.3. Algebraic distance between the CLL and straight lines between points of maximum curvature

The algebraic distance between the CLL and the straight lines drawn between the points of maximum curvature (*i.e.*, the maximum length of a line that perpendicularly intersects both the CLL and each straight line) was calculated in MATLAB for each of the three datasets. In both

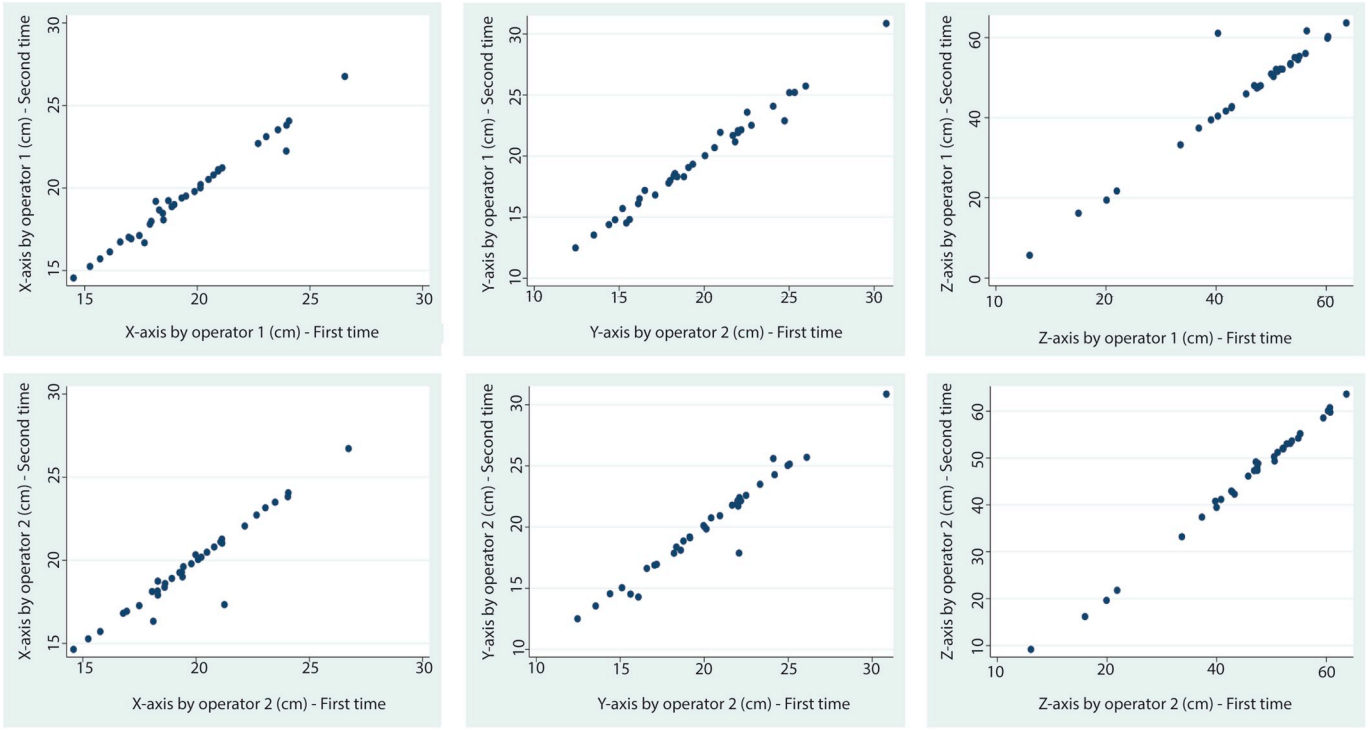

Fig. 4. Two-way scatter plots of intra-observer correlations for all points of maximum curvature (from both subjects with normal aortas and with thoracic aneurysms). *First row:* Intra-observer correlations between first and second assessments by operator 1. *Second row:* Intra-method correlations between first and second assessments by operator 2. *First column:* X-axis values. *Second column:* Y-axis values. *Third column:* Z-axis values.

subjects with and without thoracic aneurysms, the mean algebraic distances identified by the program were non-significantly lower than those identified visually (thoracic aneurysms: 0.0085 ± 0.0057 cm vs 0.0093 ± 0.0054 cm, CI95% −0.0038 to 0.0023 cm; $p = 0.6285$; normal aortas: 0.0073 ± 0.0050 cm vs 0.0078 ± 0.0052 cm, CI95% −0.0029 to 0.0019 cm; $p = 0.6285$). There were also no significant differences between operators in either group of subjects (thoracic aneurysms: $p = 0.6670$; normal aortas: $p = 0.7080$) (ANOVA: $F = 0.40$; $p = 0.5266$) (Table 6).

3.4. Mean curvature, tortuosity index and curvature-length index analyzed by program

To further characterize the geometry of thoracic aneurysms, we explored different indicators of aortic curvature and their association with the presence of aneurysms. There was no association between the presence of thoracic aneurysms and the median values of the aortic curvature. Though the tortuosity index was slightly higher in thoracic aneurysms, this association was non-significant. However, the aortic curvature-length index was significantly higher in thoracic aneurysms as compared to normal aortas (Table 7).

4. Discussion

In this study we present an automated program capable of objectively and reliably identifying aortic points of maximum curvature and calculating aortic angles in both subjects with and without aneurysmal disease.

The first important finding in our study is that our custom program can identify aortic points of maximum curvature with a high correlation, reliability and agreement with visual assessment methods, and that this can be done in both subjects with normal aortas or with thoracic aneurysms. We believe this is important since a clinically useful measure of the aortic curvature should be able to reflect the clinician's subjective assessment. Our results show appropriate inter-observer and intra-observer correlation for visual assessment measurements, suggesting that these measurements are adequate means of comparison to assess our program against.

A second finding is that the aortic angles calculated from the points of maximum curvature identified by our custom program showed a very low to moderate inter-method correlation and reliability and increased inter-method variability on agreement plots. Additionally, the value of these angles tended to be slightly higher than the value of the aortic angles calculated from the points of maximum curvature identified by visual assessment (3.3% higher for normal aortas and 5.8% higher for thoracic aneurysms), though these differences were non-significant. These discrepancies between the values of aortic angles calculated from the points of maximum curvature identified by different methods –despite apparent correlation, reliability and agreement among the points of maximum curvature identified by different methods– warrants explaining. This finding could possibly be related to a slightly higher precision in the identification of points of maximum curvature using the custom program, which is often more objective and reproducible since it follows a mathematical algorithm. This assumption is supported by the fact that the algebraic distances between the CLL and the straight lines identified by the custom program tended to be smaller than those identified by visual assessment, though this difference was not statistically significant. If these assumptions were true, even small differences in the location of points of maximum curvature could be amplified into larger differences between the angles created by these points. Despite these discrepancies, the range of values of all the aortic angles reported in our study are consistent with findings from other research groups [13]. The inter-observer reliability was adequate and within the range of other validated methods for measuring aortic angles in patients with aneurysms, suggesting once again that these measurements are appropriate means of comparison to assess our program against [11]. The correlation and reliability of the aortic angles of the normal aortas evaluated in our study overall seem slightly lower than those of the aortas with thoracic aneurysms. This may be due to the fact that aortas with thoracic aneurysms have more straight segments and sharper

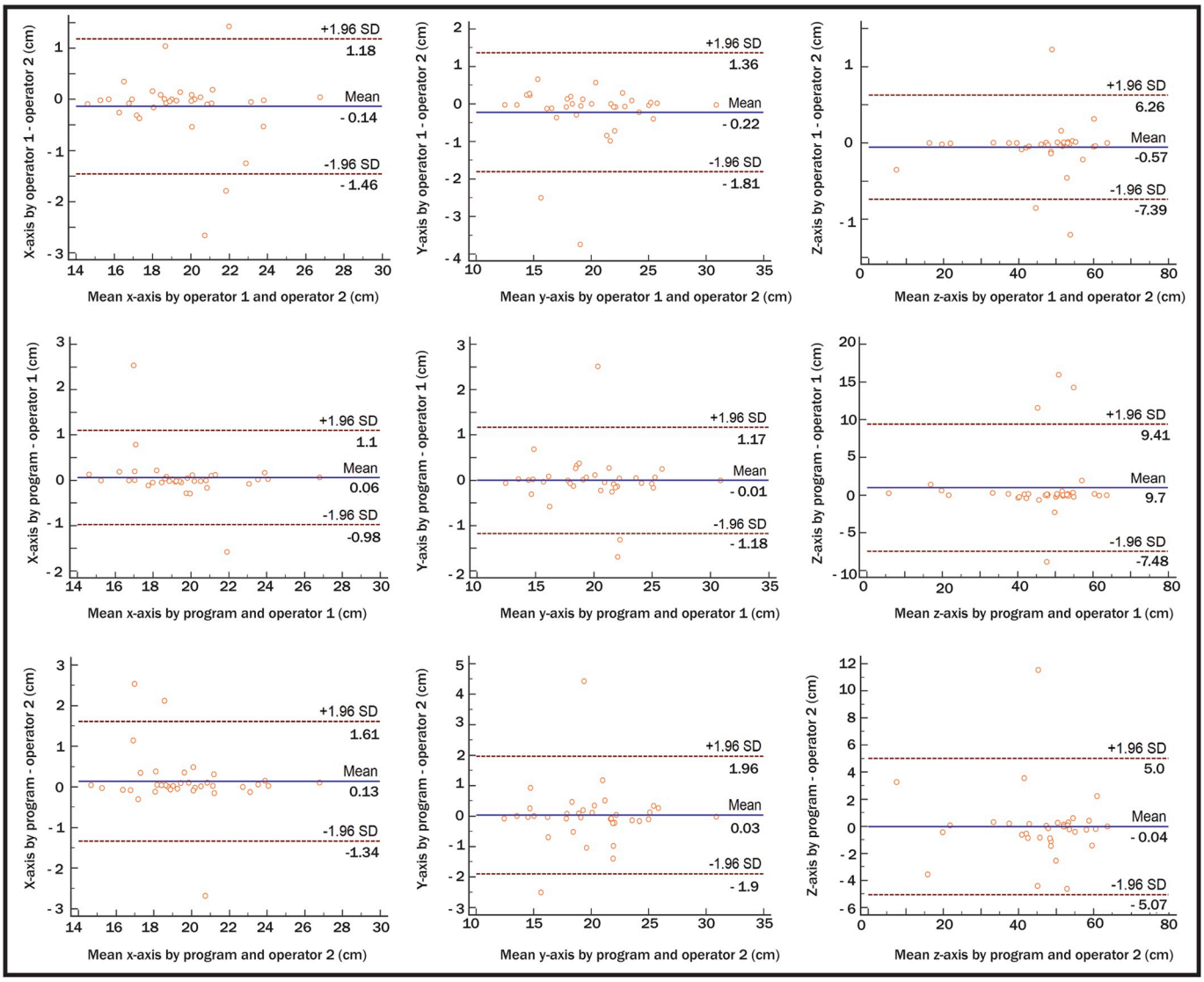

Fig. 5. Bland-Altman plots of inter-observer and inter-method agreement for all points of maximum curvature (from both subjects with normal aortas and with thoracic aneurysms). *First row:* Inter-observer agreement between operators 1 and 2. *Second row:* Inter-method agreement between program and operator 1. *Third row:* Inter-method agreement between program and operator 2. *First column:* X-axis values. *Second column:* Y-axis values. *Third column:* Z-axis values.

angles than normal aortas with a smooth curvature. These differences among aorta types could possibly lead to a more consistent identification of the points of maximum curvature in aortas with thoracic aneurysms than in normal aortas, leading to higher correlations and reliability once these differences are amplified into the angles created by these points.

The last important finding in this study is that the method used by the custom program to identify points of maximum curvature (*i.e.*, plotting curvature over position) also permits additional analyses that can help characterize the geometry of thoracic aneurysms. In this sense, the curvature-length index showed significantly different values between normal aortas and thoracic aneurysms, while more traditional indicators such as the aortic curvature and the tortuosity index did not. Classic geometric changes caused by aortic aneurysms are increased aortic tortuosity, both regionally and globally, and aortic elongation [28]. These morphometric parameters may be relevant not only in the diagnosis and characterization of aortic aneurysms, but also may also have prognostic value [29,30]. Since the tortuosity index is a measure of only global tortuosity, it may disregard regional features, therefore having poor discriminative value for identifying thoracic aneurysms [33]. The aortic curvature, on the other hand, being the integral of the CLL curvature as a function of the length of the aorta divided by the length of the aorta, can identify both global and regional increases in aortic curvature [33]. However, since this indicator indexes the CLL curvature to the total length of the aorta, it may overlook at aortic elongation as a relevant feature of thoracic aneurysms. This may be especially relevant for thoracic aneurysms, since both longitudinal and circumferential deformations throughout the aorta during the cardiac cycle are largest in the ascending aorta [31]. The only indicator evaluated in this study able to take into account both aortic elongation and increases in aortic curvatures, regional and global, is the curvature-length index. This measure is therefore an interesting candidate to explore in larger studies with predictive models of endoprosthesis complications.

Several methods have been proposed to translate clinician's intuitive interpretation of the thoracic aortic curvature into a specific metric, without reaching consensus as to which would be more appropriate and, in many cases, relying on global measures of aortic curvature or on geometric assumptions. To determine the curvature of the aortic arch in 3D reconstructions of CT scans, Chiu et al. fitted an imaginary circle to a 60-mm arc segment defined by the apex of the aorta (*i.e.*, the highest point along the centerline) and two points that were 30 mm proximal or distal to the apex along the centerline [12]. However, this geometric assumption may not be adequate for many pathological configurations

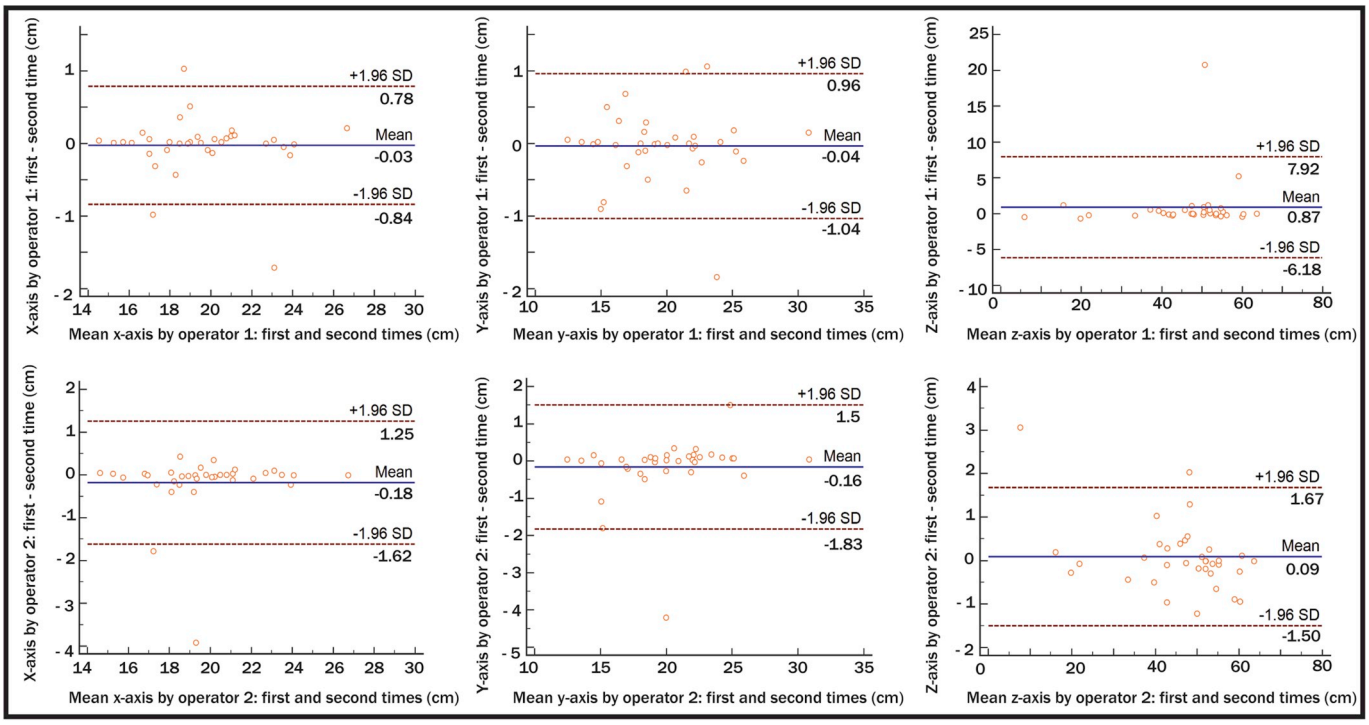

Fig. 6. Bland-Altman plots of intra-observer agreement for all points of maximum curvature (from both subjects with normal aortas and with thoracic aneurysms). *First row:* Intra-observer agreement between first and second assessments by operator 1. *Second row:* Intra-method agreement between first and second assessments by operator 2. *First column:* X-axis values. *Second column:* Y-axis values. *Third column:* Z-axis values.

Table 3
Assessment of inter-observer and inter-method reliability of points of maximum curvature with repeatability coefficients (RC) and interclass correlation coefficients (ICC) in subjects with normal aortas and with thoracic aneurysms. ‖ Difference presented as operator 1 – operator 2. ⌈ Difference presented as program – mean visual assessment. Data within parenthesis represent the 95% confidence interval. Data within brackets reflect the percentage of the mean of the first measurement.

		x-axis		y-axis		z-axis	
		RC (cm)	ICC	RC (cm)	ICC	RC (cm)	ICC
Inter-observer‖	Normal	2.81 [15.5%] (1.47–4.57)	0.997 (0.991–0.999)	3.58 [17.4%] (2.91–4.36)	0.999 (0.998–0.999)	6.38 [14.5%] (5.06–7.89)	0.999 (0.997–0.999)
	Aneurysm	1.93 [9.2%] (1.43–2.53)	0.968 (0.911–0.989)	2.38 [12.3%] (1.78–3.12)	0.983 (0.950–0.994)	3.42 [16.4%] (2.52–4.82)	0.898 (0.710–0.964)
Inter-method⌈	Normal	3.16 [17.0%] (2.62–3.76)	0.857 (0.628–0.945)	4.19 [20.8%] (3.26–5.49)	0.931 (0.821–0.973)	9.87 [22.0%] (6.57–12.79)	0.87 (0.705–0.956)
	Aneurysm	2.97 [14.3%] (1.86–3.72)	0.932 (0.810–0.976)	4.51 [23.0%] (3.12–6.25)	0.972 (0.919–0.990)	9.37 [19.4%] (6.23–12.58)	0.969 (0.912–0.989)

of the aortic arch, especially when the sharpest curvature is proximal or distal to the apex, as usually occurs with thoracic aneurysms. It also represents a global measure of the aortic curvature and therefore it may miss regional angulations that could be clinically relevant. Malkawi et al. measured the aortic arch angulation at the level of the left subclavian artery as a convenience reference point in 3D reconstructions of the CT scans of subjects undergoing TEVAR [13]. The aortic angulation at this point was defined as the angle formed by the bisectors of two lines: the line formed by the distance between the left subclavian artery and the brachiocephalic artery and a line perpendicular to the CLL at an equal distance distal to the left subclavian artery. Following a similar approach, in a mathematical model assessing risk factors for the formation of thoracic aorta aneurysms, Poullis et al. calculated the aortic curvature as the angle formed by a line perpendicular to the plane of the aortic valve and a line perpendicular to the cross section at the origin of the innominate artery. One of the drawbacks of these methods is that these convenience reference points may not adequately represent the entire aortic curvature in certain pathological situations. Agnoletti et *al.* measured the angle of the aortic arch on a two-dimensional (2D) lateral view of an aortogram in children who had undergone an arterial switch operation for transposition of great vessels [14]. The aortic arch angle was considered as the angle at the highest point of the aortic arch formed by the intersection of the straight lines that pass through the midpoints of the ascending and the descending aorta. The 2D assessment of the aortic arch angle in this method has important limitations, since 3D curvatures are often unapparent in 2D analyses [32]. Following an approach similar to ours, Kotelis et *al.* fitted cubic polynomials to the 3D CLL within a certain range of interest and computed the local centerline curvature using first- and second-order partial derivatives of the fitted polynomials [33]. These authors also measured the thoracic aorta's conicity as the difference between the maximum aortic diameters 1 cm proximal and 1 cm distal to a region of interest. Nakatamari et al. measured the curvature index of the aortas of patients undergoing TEVAR as the inverse radius of curvature of the CLL measured at 1-cm intervals [5]. Boufi et al. and Chen et al. analyzed the tortuosity index of the aortic arch of either healthy subjects or patients undergoing TEVAR. Both authors used the tortuosity index as an indicator of global aortic curvature, calculating the ratio of the distance along the CLL between two points divided by the straight distance between these two points [18,20,34]. On the contrary, Ueda et al. measured the tortuosity

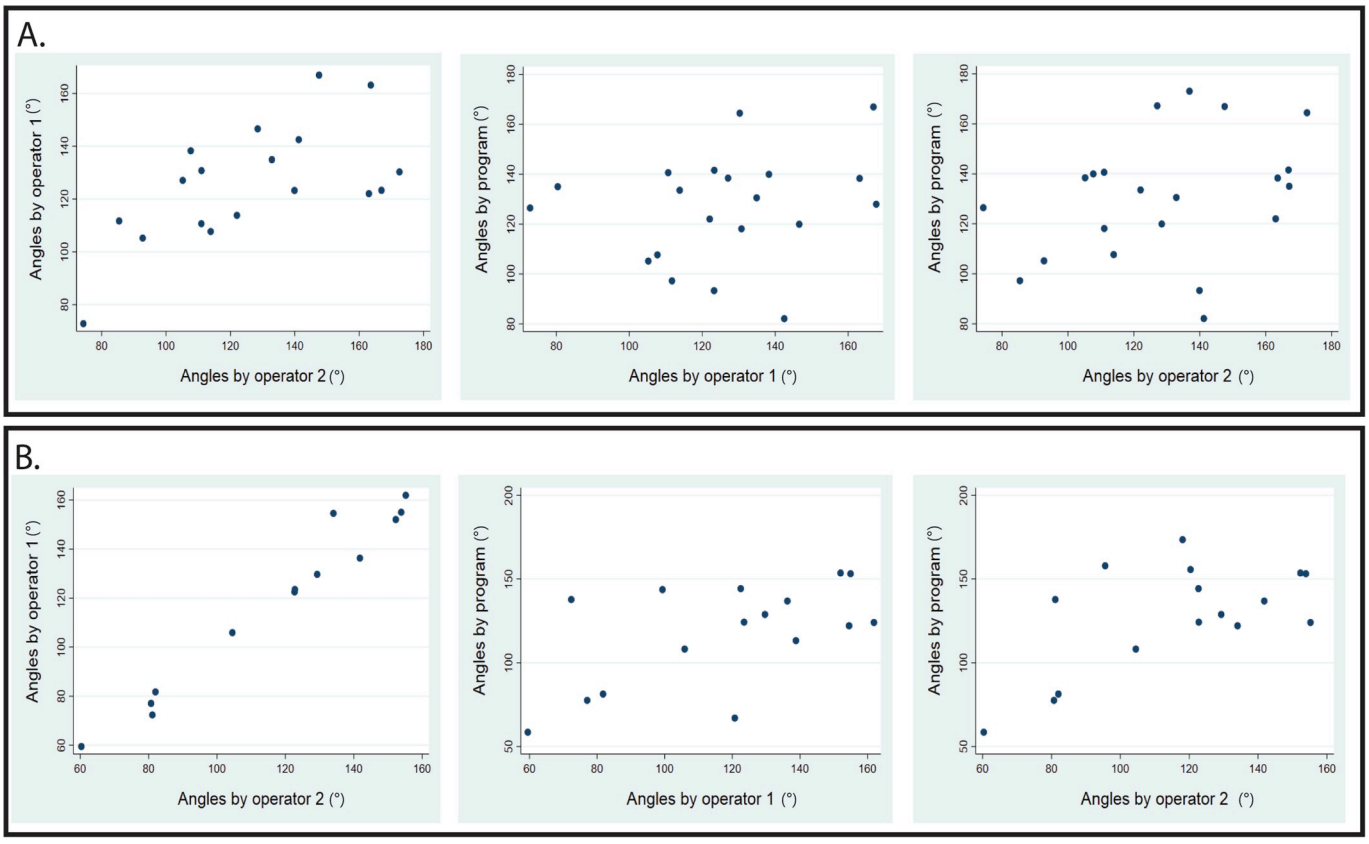

Fig. 7. Two-way scatter plots of inter-observer and inter-method correlations for aortic angles from subjects with normal aortas (A) and with thoracic aneurysms (B). *First column:* Inter-observer correlations between operators 1 and 2. *Second column:* Inter-method correlations between program and operator 1. *Third column:* Inter-method correlations between program and operator 2.

index of patients undergoing TEVAR as the sum of curvature values greater than 0.2 cm^{-1} in the segments of interest [6]. We believe these morphometric parameters calculated with mathematical algorithms applied to automatically-generated CLL of the thoracic aorta are a more accurate approximation to the aortic curvature since they take into account the 3D nature and the anatomical complexity of the aorta, making less geometric assumptions. Finally, the aortic curvature can be measured through visual assessment, which is the technique used in daily clinical practice [35]. However, visual methods are usually cumbersome and time-consuming. Additionally, since visual assessment methods are subjective they may have limited reliability [35,36]. To our knowledge this is the first study to systematically compare visual assessment measures of the thoracic aortic curvature of normal and aneurysmatic aortas with 3D CLL curvature measures.

The reason so much effort from the scientific community has been put into characterizing this parameter using so many different indexes is the increasing evidence indicating that the aortic curvature or tortuosity or angulation or conicity may be associated with post-procedural complications after TEVAR [5–8]' [37]. The rationale behind this association is that the more tortuous the thoracic aorta, the more likely there could be an incomplete stent-graft apposition with the aortic wall, thus producing endoleaks [38]. Additionally, as the curvature of the ascending aorta increases towards the aortic arch, the forces conferred on the aortic wall secondary to blood flow also increase, promoting vessel dilation and possibly endoleak formation [39]. An accurate assessment of the anatomical curvature of the thoracic aorta therefore seems to be essential for appropriate endoprosthesis sizing. There is evidence that the location and tortuosity of the aorta may be related to the risk of endoleak formation after thoracic EVAR [5,6]. The availability of information on the precise location of an aortic angulation could determine if the length of a non-angulated neck is long enough to allow a complete apposition of a stent-graft, thus preventing endoleaks or stent-graft collapse [40]. The magnitude of aortic angles, especially in the proximal and distal neck, may also increase the risk of endoleaks [37,41]. In a small retrospective study of 57 patients, a higher conicity in the proximal landing zone of the aorta has been associated with an increase in the type Ia endoleak rate after TEVAR, while a smaller aortic arch curvature radius has been associated with an incomplete apposition of the stent-graft to the aortic wall, called "bird-beak" configuration [32]. In a small prospective study of 40 patients with thoracic aneurysms, Ueda 2011 found an association between type I and III endoleak formation and the value of the tortuosity index at different aortic locations. These results suggest that the curvature of the thoracic aorta may be an important feature for the planning endovascular repair, since it may influence the stability of the endograft fixation. Therefore, an objective quantification of the curvature of the thoracic aorta could contribute to risk stratification to predict the formation of endoleaks after TEVAR. A robust prediction method like this could be clinically helpful in assessing the performance of devices in clinical trials and guide routine clinical decision-making [42].

Our study has several limitations. First, since it is a validation study, the number of subjects is small. A larger study with more human subjects would increase the external validity of our conclusions. Second, our results are mainly descriptive, therefore their clinical implications remain unknown. To assess the clinical value of the points of maximum curvature identified by our custom program, a large prospective clinical study exploring complications after TEVAR would be necessary. Third, since the aortic angles were calculated from three unevenly distributed points, the distance between the center point and the other two points would have an influence on how much variations in the position of the extreme points are amplified on calculating the aortic angles. That is, the smaller the distance between the points, the larger the influence of these

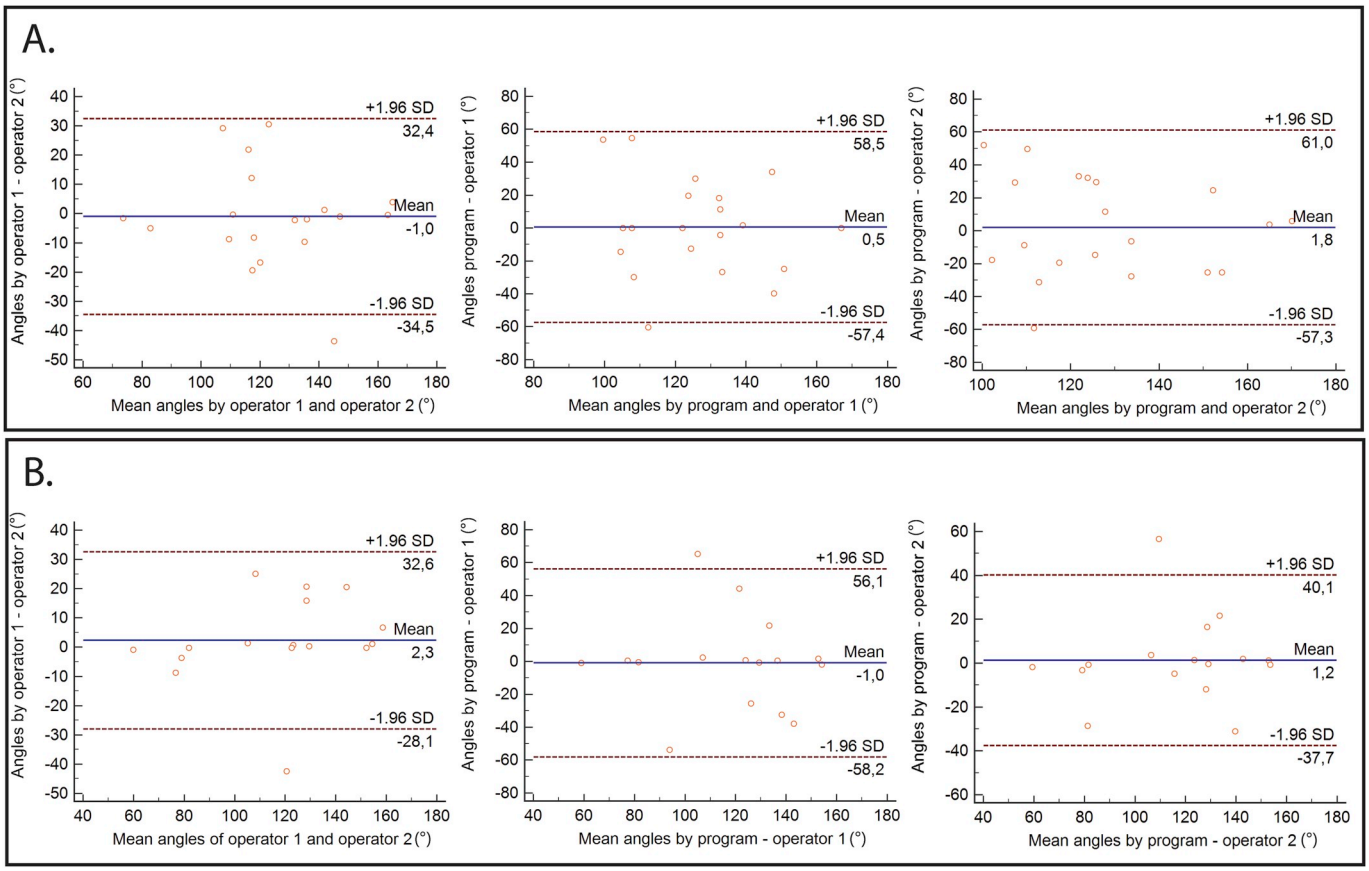

Fig. 8. Bland-Altman plots of inter-observer and inter-method agreement for aortic angles from subjects with normal aortas (A) and with thoracic aneurysms (B). *First column:* Inter-observer agreement between operators 1 and 2. *Second column:* Inter-method agreement between program and operator 1. *Third column:* Inter-method agreement between program and operator 2.

Table 4
Aortic angles between straight lines joining the points of maximum curvature identified by each operator/method in subjects with normal aortas and with thoracic aneurysms. SD: standard deviation. Program vs operators: thoracic aneurysms: $p = 0.4282$; normal aortas: $p = 0.5281$. Operator 1 vs operator 2: thoracic aneurysms: $p = 0.7104$; normal aortas: $p = 0.8374$. ANOVA: $F = 0.49$; $p = 0.6114$. Hypotheses testing was conducted using a Bonferroni-adjusted alpha level of 0.0125 in each test (0.05/4).

	Type of aorta	Mean (°)	SD (°)
Operator 1	Normal	125.9	25.2
	Aneurysm	118.2	32.4
Operator 2	Normal	129.1	28.3
	Aneurysm	115.9	29.2
Program	Normal	131.8	24.7
	Aneurysm	124.3	32.8

Table 6
Algebraic distance between the CLL and straight lines between points of maximum curvature identified by each operator/method in subjects with normal aortas and with thoracic aneurysms. SD: standard deviation. Program vs operators: thoracic aneurysms: $p = 0.6285$; normal aortas: $p = 0.6285$. Operator 1 vs operator 2: thoracic aneurysms: $p = 0.6670$; normal aortas: $p = 0.7080$. ANOVA: $F = 0.40$; $p = 0.5266$. Hypotheses testing was conducted using a Bonferroni-adjusted alpha level of 0.0125 in each test (0.05/4).

	Type of aorta	Algebraic distance (cm)	SD (cm)
Operator 1	Normal	0.0075	0.0052
	Aneurysm	0.0091	0.0049
Operator 2	Normal	0.0077	0.0054
	Aneurysm	0.0094	0.0059
Program	Normal	0.0073	0.0050
	Aneurysm	0.0085	0.0057

Table 5
Assessment of inter-observer and inter-method variability and reliability of aortic angles with mean differences, repeatability coefficients (RC) and interclass correlation coefficients (ICC) in subjects with normal aortas and with thoracic aneurysms.‖ Difference presented as operator 1 – operator 2. ⌈ Difference presented as program – median visual assessment. SE: standard error. 95%CI: 95% confidence interval. Data within brackets reflect the percentage of the mean of the first measurement.

	Type of aorta	Mean Difference (°)	SE (°)	95%CI (°)	RC	95%CI	ICC	95%CI
Inter-observer‖	Normal	−3.1 [-2.5%]	8.4	−20.1 to 13.8	32.6 [25.9%]	24.8 to 47.7	0.87	0.66 to 0.95
	Aneurysm	2.3 [4.4%]	10.9	−20.0 to 24.5	29.7 [25.1%]	22.1 to 45.2	0.93	0.81 to 0.98
Inter-method⌈	Normal	4.3 [3.3%]	6.7	−9.2 to 17.8	54.9 [41.6%]	42.4 to 78.5	0.49	−0.26 to 0.79
	Aneurysm	7.2 [5.8%]	9.1	−11.0 to 25.5	45.0 [36.2%]	33.5 to 68.5	0.82	0.48 to 0.94

Table 7
Aortic curvature, tortuosity and curvature-length-index (CLI) of normal aortas and thoracic aneurysms. Data are presented as median and interquartile range (IQR) and analyzed by Wilcoxon (Mann-Whitney U) test.

	Normal aortas	IQR	Thoracic aneurysms	IQR	p
Curvature - cm^{-1}	0.16	[0.15–0.17]	0.17	[0.17–0.19]	0.0864
Tortuosity index	2.2	[2.1–2.6]	3.3	[2.8–3.3]	0.0500
CLI	**5.4**	**[5.2–5.5]**	**6.8**	**[6.4–8.1]**	**0.0143**

variations on aortic angle calculations. This limitation is inherent to our method and must be acknowledged. Forth, since the tortuosity of the aorta can change with age [43], we chose a middle-aged population for this validation study. This choice could have limitations for interpreting the CT scans of both elder patients with degenerative thoracic aneurysms and of younger patients with thoracic aneurysms related to specific conditions, such as a bicuspid aortic valve or Marfan syndrome. We recognize that this a limitation that needs to be addressed in larger studies with a wider age-span.

The clinical relevance of our findings lies in the lack of inter-method correlation and agreement for aortic angles, while inter-method correlation and agreement are appropriate for points of maximum curvature. We believe that this is due to the fact that operators rely only on their clinical training and intuition for identifying points of maximum curvature. Though their performance may be high, they can make small errors that are amplified into larger errors on calculating the aortic angles. On the contrary, since the program identifies the points of maximum curvature with a mathematical algorithm, it is both objective and reproducible. The apparently small additional precision added by the program in identifying the points of maximum curvature is magnified on using these points to calculate the aortic angles. Therefore, if the predictive value of aortic angles for the development of endoleaks after TEVAR were eventually established, the clinical value of our program for calculating aortic angles would be considerable.

Overall, we believe our program for identifying points of maximum curvature is promising because it shows good agreement with points identified by physicians, without relying on geometric assumptions and is objective, automatic and reproducible. Since it only requires the manual selection of the first and last lumen points to create the CLL, we believe this method could reduce potential error and user time. Lastly, our automated program could be used in the preoperative workup of patients with thoracic aneurysms to identify patients at risk for endoleak formation after TEVAR, without the inaccuracies, inter-observer variance and prolonged user time of visual assessment.

Funding

This work was supported by the 2016 ECOS-SUD grant [project number A16S03] between the Ministerio de Ciencia y Tecnología from Argentina and the Ministère de l'Education Nationale et de la Recherche from France, by the PICT2015-2168 grant from the Agencia Nacional de Promocion Científica y Tecnológica from Argentina, and by the Universidad de Buenos Aires travel grants from Argentina [number EXP-UBA 32.318/2018].

Conflicts of interest

None declared.

Appendix A. Supplementary data

Supplementary data to this article can be found online at https://doi.org/10.1016/j.compbiomed.2019.103440.

References

[1] S.A. Goldstein, A. Evangelista, S. Abbara, A. Arai, F.M. Asch, L.P. Badano, et al., Multimodality imaging of diseases of the thoracic aorta in adults: from the American society of echocardiography and the european association of cardiovascular imaging, J. Am. Soc. Echocardiogr. 28 (2015) 119e82, https://doi.org/10.1016/j.echo.2014.11.015.
[2] V. Riambau, D. Böckler, J. Brunkwall, P. Cao, R. Chiesa, G. Coppi, et al., Editor's choice–management of descending thoracic aorta diseases: clinical practice guidelines of the European Society for Vascular Surgery (ESVS), Eur. J. Vasc. Endovasc. Surg. 53 (1) (2017) 4–52, https://doi.org/10.1016/j.ejvs.2016.06.005.
[3] J.N. Bowman, D. Silverberg, S. Ellozy, V. Teodorescu, H. Poblete, M. Marin, et al., The role of anatomic factors in predicting success of endovascular repair of thoracic aortic aneurysms, Vasc. Endovasc. Surg. 44 (2) (2010) 101–104, https://doi.org/10.1177/1538574409347392.
[4] G. Piffaretti, G. Mariscalco, C. Lomazzi, N. Rivolta, F. Riva, M. Tozzi, et al., Predictive factors for endoleaks after thoracic aortic aneurysm endograft repair, J. Thorac. Cardiovasc. Surg. 138 (4) (2009) 880–885, https://doi.org/10.1016/j.jtcvs.2009.02.024.
[5] H. Nakatamari, T. Ueda, F. Ishioka, B. Raman, K. Kurihara, G.D. Rubin, Discriminant analysis of native thoracic aortic curvature: risk prediction for endoleak formation after thoracic endovascular aortic repair, J. Vasc. Interv. Radiol. 22 (7) (2011) 974–979, https://doi.org/10.1016/j.jvir.2011.02.031.
[6] T. Ueda, H. Takaoka, B. Raman, J. Rosenberg, G.D. Rubin, Impact of quantitatively determined native thoracic aortic tortuosity on endoleak development after thoracic endovascular aortic repair, Am. J. Roentgenol. 197 (6) (2011) W1140–W1146, https://doi.org/10.2214/AJR.11.6819.
[7] D.Y. Sze, M.A. Van Den Bosch, M.D. Dake, D.C. Miller, L.V. Hofmann, R. Varghese, Factors portending endoleak formation after thoracic aortic stent-graft repair of complicated aortic dissection, Circulation: Cardiovasc. Interv. 2 (2) (2009) 105–112, https://doi.org/10.1161/CIRCINTERVENTIONS.108.819722.
[8] H.E. Altnji, B. Bou-Saïd, H. Walter-Le Berre, Morphological and stent design risk factors to prevent migration phenomena for a thoracic aneurysm: a numerical analysis, Med. Eng. Phys. 37 (1) (2015) 23–33, https://doi.org/10.1016/j.medengphy.2014.09.017.
[9] J. Yunoki, T. Kuratani, Y. Shirakawa, K. Torikai, K. Shimamura, K. Kin, et al., Mid-term results of endovascular treatment with the Gore TAG device for degenerative descending thoracic aortic aneurysms, Gen. Thorac. Cardiovasc. Surg. 63 (1) (2015) 38–42, https://doi.org/10.1007/s11748-014-0436-4.
[10] N.F. Oliveira, F.M. Bastos Gonçalves, J.P. de Vries, K.H. Ultee, D.A. Werson, S. E. Hoeks, et al., Mid-Term results of EVAR in severe proximal aneurysm neck angulation, Eur. J. Vasc. Endovasc. Surg. 49 (1) (2015) 19–27, https://doi.org/10.1016/j.ejvs.2014.10.001.
[11] J.W. van Keulen, F.L. Moll, J.L. Tolenaar, H.J. Verhagen, J.A. van Herwaarden, Validation of a new standardized method to measure proximal aneurysm neck angulation, J. Vasc. Surg. 51 (4) (2010 Apr) 821–828, https://doi.org/10.1016/j.jvs.2009.10.114.
[12] P. Chiu, H.P. Lee, S.K. Venkatesh, P. Ho, Anatomical characteristics of the thoracic aortic arch in an Asian population, Asian Cardiovasc. Thorac. Ann. 21 (2) (2013) 151–159, https://doi.org/10.1177/0218492312449637.
[13] A.H. Malkawi, R.J. Hinchliffe, M. Yates, P.J. Holt, I.M. Loftus, M.M. Thompson, Morphology of aortic arch pathology: implications for endovascular repair, J. Endovasc. Ther. 17 (4) (2010) 474–479, https://doi.org/10.1583/10-3067.1.
[14] G. Agnoletti, P. Ou, D.S. Celermajer, Y. Boudjemline, D. Marini, D. Bonnet, et al., Acute angulation of the aortic arch predisposes a patient to ascending aortic dilatation and aortic regurgitation late after the arterial switch operation for transposition of the great arteries, J. Thorac. Cardiovasc. Surg. 135 (3) (2008) 568–572, https://doi.org/10.1016/j.jtcvs.2007.10.020.
[15] A. Kaladji, A. Lucas, G. Kervio, P. Haigron, A. Cardon, Sizing for endovascular aneurysm repair: clinical evaluation of a new automated three-dimensional software, Ann. Vasc. Surg. 24 (7) (2010) 912–920, https://doi.org/10.1016/j.avsg.2010.03.018.
[16] A. Kaladji, A. Cardon, B. Laviolle, J.F. Heautot, G. Pinel, A. Lucas, Evolution of the upper and lower landing site after endovascular aortic aneurysm repair, J. Vasc. Surg. 55 (1) (2012) 24–32, https://doi.org/10.1016/j.jvs.2011.07.067.
[17] A. Kaladji, A. Cardon, I. Abouliatim, B. Campillo-Gimenez, J.F. Heautot, J. P. Verhoye, Preoperative predictive factors of aneurysmal regression using the reporting standards for endovascular aortic aneurysm repair, J. Vasc. Surg. 55 (5) (2012) 1287–1295, https://doi.org/10.1016/j.jvs.2011.11.122.
[18] C.K. Chen, I.P. Liang, H.T. Chang, W.Y. Chen, I.M. Chen, M.H. Wu, M.H. Sheu, C. C. Shih, Impact on outcomes by measuring tortuosity with reporting standards for thoracic endovascular aortic repair, J. Vasc. Surg. 60 (4) (2014) 937–944.
[19] E.L. Chaikof, J.D. Blankensteijn, P.L. Harris, G.H. White, C.K. Zarins, V. M. Bernhard, J.S. Matsumura, J. May, F.J. Veith, M.F. Fillinger, R.B. Rutherford, Reporting standards for endovascular aortic aneurysm repair, J. Vasc. Surg. 35 (5) (2002) 1048–1060.
[20] C.K. Chen, H.P. Chou, C.Y. Guo, H.T. Chang, Y.Y. Chang, I.M. Chen, M.H. Wu, C. C. Shih, Interobserver and intraobserver variability in measuring the tortuosity of the thoracic aorta on computed tomography, J. Vasc. Surg. 68 (4) (2018) 1183–1192, https://doi.org/10.1016/j.jvs.2018.01.047, e1.
[21] A.G. Asuero, A. Sayago, A.G. Gonzalez, The correlation coefficient: an overview, Crit. Rev. Anal. Chem. 36 (1) (2006) 41–59.
[22] J.M. Bland, D.G. Altman, Statistical methods for assessing agreement between two methods of clinical measurement, Lancet 1 (1986) 307–310.
[23] D. Giavarina, Understanding Bland Altman analysis. *Biochemia medica*, Biochem. Med. 25.2 (2015) 141–151.

[24] S. Vaz, T. Falkmer, A.E. Passmore, R. Parsons, P. Andreou, The case for using the repeatability coefficient when calculating test–retest reliability, PLoS One 8 (9) (2013) e73990, https://doi.org/10.1371/journal.pone.0073990.
[25] P.E. Shrout, J.L. Fleiss, Intraclass correlations: uses in assessing rater reliability, Psychol. Bull. 86 (2) (1979) 420.
[26] T.K. Koo, M.Y. Li, A guideline of selecting and reporting intraclass correlation coefficients for reliability research, J. Chiropr. Med. 15 (2016) 155–163.
[27] R Core Team, R: A Language and Environment for Statistical Computing, R Foundation for Statistical Computing, Vienna, Austria, 2013. http://www.R-project.org/.
[28] T. Kruger, R. Sandoval Boburg, M. Lescan, A. Oikonomou, W. Schneider, L. Vohringer, et al., Aortic elongation in aortic aneurysm and dissection: the Tubingen Aortic Pathoanatomy (TAIPAN) project, Eur. J. Cardiothorac. Surg. 54 (2018) 26–33, https://doi.org/10.1093/ejcts/ezx503.
[29] J.A. Elefteriades, E.A. Farkas, Thoracic aortic aneurysm: clinically pertinent controversies and uncertainties, J. Am. Coll. Cardiol. 55 (9) (2010) 841–857.
[30] S. Pappu, A. Dardik, H. Tagare, R.J. Gusberg, Beyond fusiform and saccular: a novel quantitative tortuosity index may help classify aneurysm shape and predict aneurysm rupture potential, Ann. Vasc. Surg. 22 (1) (2008) 88–97.
[31] H.W.L. de Beaufort, F.J.H. Nauta, M. Conti, E. Cellitti, C. Trentin, E. Faggiano, G.H. W. van Bogerijen, C.A. Figueroa, F.L. Moll, J.A. van Herwaarden, F. Auricchio, Extensibility and distensibility of the thoracic aorta in patients with aneurysm, Eur. J. Vasc. Endovasc. Surg. 53 (2) (2017) 199–205, https://doi.org/10.1016/j.ejvs.2016.11.018.
[32] B. Reutersberg, B. Haller, J. Mariss, H.H. Eckstein, S. Ockert, Measurements after image post-processing are more precise in the morphometric assessment of thoracic aortic aneurysms: an intermodal and intra-observer evaluation, Eur. J. Vasc. Endovasc. Surg. 52 (4) (2016) 509–517.
[33] D. Kotelis, C. Brenke, S. Wörz, F. Rengier, K. Rohr, H.U. Kauczor, D. Böckler, H. von Tengg-Kobligk, Aortic morphometry at endograft position as assessed by 3D image analysis affects risk of type I endoleak formation after TEVAR, Langenbeck's Arch. Surg. 400 (4) (2015) 523–529, https://doi.org/10.1007/s00423-015-1291-1.
[34] M. Boufi, C. Guivier-Curien, A.D. Loundou, V. Deplano, O. Boiron, K. Chaumoitre, V. Gariboldi, Y.S. Alimi, Morphological analysis of healthy aortic arch, Eur. J. Vasc. Endovasc. Surg. 53 (5) (2017) 663–670, https://doi.org/10.1016/j.ejvs.2017.02.023.
[35] M.F. Fillinger, J. Racusin, R.K. Baker, J.L. Cronenwett, A. Teutelink, M. L. Schermerhorn, R.M. Zwolak, R.J. Powell, D.B. Walsh, E.M. Rzucidlo, Anatomic characteristics of ruptured abdominal aortic aneurysm on conventional CT scans: implications for rupture risk, J. Vasc. Surg. 39 (6) (2004) 1243–1252, https://doi.org/10.1016/j.jvs.2004.02.025.
[36] K. Singh, B.K. Jacobsen, S. Solberg, K.H. Bonaa, S. Kumar, R. Bajic, et al., Intra- and interobserver variability in the measurements of abdominal aortic and common iliac artery diameter with computed tomography. The Tromso Study, Eur. J. Vasc. Endovasc. Surg. 25 (2003) 399–407.
[37] J. Yunoki, T. Kuratani, Y. Shirakawa, K. Torikai, K. Shimamura, K. Kin, et al., Mid-term results of endovascular treatment with the Gore TAG device for degenerative descending thoracic aortic aneurysms, Gen. Thorac. Cardiovasc. Surg. 63 (1) (2015) 38–42, https://doi.org/10.1007/s11748-014-0436-4.
[38] T. Ueda, D. Fleischmann, M.D. Dake, G.D. Rubin, D.Y. Sze, Incomplete endograft apposition to the aortic arch: bird-beak configuration increases risk of endoleak formation after thoracic endovascular aortic repair, Radiology 255 (2010) 645–652, https://doi.org/10.1148/radiol.10091468.
[39] M.P. Poullis, R. Warwick, A. Oo, R.J. Poole, Ascending aortic curvature as an independent risk factor for type A dissection, and ascending aortic aneurysm formation: a mathematical model, Eur. J. Cardiothorac. Surg. 33 (6) (2008) 995–1001, https://doi.org/10.1016/j.ejcts.2008.02.029.
[40] L. Canaud, P. Alric, P. Desgranges, J. Marzelle, C. Marty-Ané, J.P. Becquemin, Factors favoring stent-graft collapse after thoracic endovascular aortic repair, J. Thorac. Cardiovasc. Surg. 139 (5) (2010) 1153–1157, https://doi.org/10.1016/j.jtcvs.2009.06.017.
[41] H.E. Altnji, B. Bou-Saïd, H. Walter-Le Berre, Morphological and stent design risk factors to prevent migration phenomena for a thoracic aneurysm: a numerical analysis, Med. Eng. Phys. 37 (1) (2015) 23–33, https://doi.org/10.1016/j.medengphy.2014.09.017.
[42] B. Rylski, M. Czerny, M. Südkamp, M. Siepe, F. Beyersdorf, The TEVAR App: a contemporary guide to thoracic endovascular aortic repair, Interact. Cardiovasc. Thorac. Surg. 22 (2016) 228–230.
[43] A.M. Tawfik, D.M. Sobh, B. Gadelhak, H.M. Sobh, N.M. Batouty, The effect of age and gender on tortuosity of the descending thoracic Aorta, Eur. J. Radiol. 110 (2019) 54–59.